Resonant coherent three-photon photoemission from Cu(001)

Aimo Winkelmann,[1,*] Wen-Chin Lin,[1] Cheng-Tien Chiang,[1] Francesco Bisio,[2,3] Hrvoje Petek,[4] and Jürgen Kirschner[1]
[1]*Max-Planck Institut für Mikrostrukturphysik, Weinberg 2, D-06120 Halle (Saale), Germany*
[2]*CNISM, Sede consorziata di Genova, via Dodecaneso 33, I-16146 Genova, Italy*
[3]*CNR-INFM LAMIA, Corso Perrone 24, I-16152 Genova, Italy*
[4]*Department of Physics and Astronomy, University of Pittsburgh, Pittsburgh, Pennsylvania 15260, USA*
(Received 23 July 2009; revised manuscript received 22 September 2009; published 20 October 2009)

We demonstrate the contribution of coherent excitation pathways in three-photon photoemission from Cu(001). We identify separate peaks in the photoelectron spectra as originating from two specific Cu *d* bands that are excited at different *k* points via the *same* unoccupied image-potential state. By model calculations we show that our experimental observations impose lower limits on the relevant Cu *d*-hole dephasing time on the order of 10–20 fs. Our findings suggest extensions to future studies in electronic structure mapping with tunable laboratory and free-electron laser sources, exploiting possible multiphoton resonances between occupied bulk and unoccupied surface states.

DOI: 10.1103/PhysRevB.80.155128 PACS number(s): 79.60.Bm

I. INTRODUCTION

The effect of quantized energy absorption by electrons[1] is at the heart of angle-resolved photoemission spectroscopy (ARPES) as the most general and widely employed method for mapping the occupied electronic structure in solids.[2,3] In the simplest picture, the incident radiation induces transitions of electrons from occupied to unoccupied single-particle states separated by the photon energy. By invoking the laws of energy and momentum conservation, the photoemission process can be applied to map the occupied band structure of solids by detecting the photoelectrons in final states above the vacuum barrier.

A generalization of the photoelectric effect can be realized by multiphoton processes induced by ultrashort laser pulses of high intensity, where the occupied initial states, the unoccupied intermediate states, and the coupling between them play a central role. Especially the technique of time-resolved two-photon photoemission (2PPE) has been used to gain information on the decay rates of electronic populations and on the survival times of coherent superpositions of states ("dephasing times").[4–6] Interferometric 2PPE measurements[6] have been used to determine dephasing times of quantum coherence at metal surfaces[7–9] and recently the control of directional surface currents was also demonstrated.[10] Also, interference in 2PPE can be observed directly if several close-lying unoccupied states are excited coherently. The 2PPE yield then can show quantum beats[11] and the decay of these beats allows us to investigate the dephasing process between the various states due to intrinsic properties of solids and scattering with the impurities.[12] More indirectly, dephasing can also be estimated from frequency domain measurements via its influence on the measured linewidths.[5] The decisive role of dephasing processes in 2PPE is also seen by the fact that in the total absence of dephasing, under certain circumstances intermediate surface states should not be observed at all because of destructive interference between different excitation pathways.[13,14]

As multiphoton photoemission experiments depend sensitively on the wave functions and energy levels of the states that are involved in the excitation, they are expected to provide band-structure information about occupied and unoccupied states in solids with high precision.[15] Because photons in the visible and UV range cannot transfer significant momentum to the electrons, such multiphoton resonances effectively proceed vertically in the electronic $E(\vec{\mathbf{k}})$ band-structure (just as optical transitions in conventional ARPES measurements) and thus can be used to determine the separation of electronic bands at specific $\vec{\mathbf{k}}$ points by looking for resonances between the multiple states coupled by the incident radiation. The linewidth and intensity of the observed signals depend on the dephasing rates in the relevant states. This is why it is important to examine the implications of coherence in optically excited solid-state systems.

In this paper we report observations of coherent multiphoton photoemission that carries information about the bulk band structure of copper by resonant excitation of electronic bulk states through unoccupied intermediate surface states. In a three-photon photoemission experiment from a Cu(001) surface, we identify separate peaks in the photoelectron spectra as originating from different initial state Cu *d* bands that are resonantly excited at different photon energies via the *same* unoccupied image-potential (IP) state. The image-potential states reside at a fixed energy for a specific surface parallel momentum and thus can provide a reliable reference level. This study builds on our previous investigations where we have demonstrated that at a Cu(001) surface, three- and even four-photon photoemission (3PPE and 4PPE) processes with clear band-structure-related features are in principle observable.[16] Using spin-resolved detection and circularly polarized light for excitation, we also demonstrated that the $n=1$ image-potential state on Cu(001) can be selectively coupled to two spin-orbit split *d* bands belonging to different components of the double-group symmetry[17] and we showed that it is possible to control this process[18] interferometrically. In this contribution, we will analyze the role of phase-preserving multiphoton excitation processes in conveying bulk band-structure information.

II. EXPERIMENTAL DETAILS

The experimental setup is the same as described before.[16,17] Compared to the previous experiments, we used

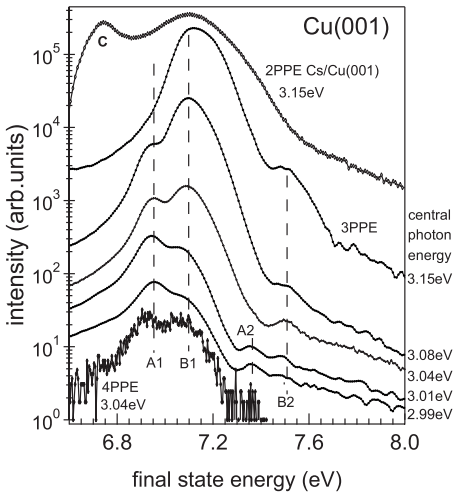

FIG. 1. Experimental spectra of the 3PPE resonance as a function of the central energy of the excitation pulse, *p*-polarized excitation (logarithmic scale). For comparison, the 2PPE spectrum from cesiated Cu(001) is shown shifted upward by $h\nu$ and the 4PPE peak is shifted downward by $h\nu$. Feature C in the 2PPE spectrum near the vacuum edge is due a background of secondary electrons which could not be further decreased. The spectra are displaced vertically for better visibility. They are not normalized with respect to the laser intensity.

the electrostatic electron energy analyzer in a higher energy resolution mode of about 50 meV as was estimated from the low-energy cutoff of the photoelectron spectra. The photoemission experiments were carried out in an ultrahigh-vacuum system (pressure $<5\times10^{-11}$ mbar). The ultrashort excitation pulses were provided by the frequency-doubled output of a self-built Ti:sapphire oscillator. The pulse central energy could be continuously varied in the range of $h\nu=2.99-3.15$ eV by tuning the phase-matching angle of the frequency-doubling 80-μm-thick β-BaB_2O_4 crystal. At the energy of $h\nu=3.07$ eV, the pulse length at the surface was $\leq$20 fs and the pulse energy $\sim$1 nJ. A clean and ordered Cu(001) surface was prepared by standard sputtering and annealing procedures. The optical plane was aligned parallel to the [100] direction. All the experiments, unless specified, were carried out at 300 K. The electrons photoemitted along the surface normal were analyzed by a cylindrical sector analyzer (Focus CSA300).

III. RESULTS

In Fig. 1, we show experimental 3PPE spectra taken for different central energies of the exciting pulse using *p*-polarized excitation. We show for comparison the 2PPE part of the spectrum on top and the 4PPE part at the bottom of Fig. 1.[16] For the 3PPE spectra, four peaks A1, B1, A2, and B2 can be identified. An analysis of the dominating double-peak structure A1 and B1 shows that this part of the spectrum can be fitted by the sum of two Gaussian peaks with widths (full width at half maximum) of 110 meV for (A1) and 130 meV for (B1) and a separation of 150 meV. Peak A1 is located at a final-state energy of 6.95 eV and peak B1 at 7.15 eV. Considering that the optical spectrum of the excitation pulses has a width of 170 meV, the resolution of the 3PPE spectrum well below the excitation linewidth in the three-photon absorption process is striking.

The peaks A1 and B1 obviously do not disperse noticeably with energy but only change their relative intensities. This relative change is connected to an underlying overall shift of intensity, which moves at the same rate as the photon energy $\Delta h\nu$.[17] This shift with $\Delta h\nu$ can be clearly seen from the position of the high-energy wings of the observed peaks. In a (generally nonresonant) three-photon photoemission process involving states with fixed energy (i.e., not dispersing with $k_\perp$), it can be expected that the position of a peak from the initial state tunes with $3\Delta h\nu$, the first intermediate state with $2\Delta h\nu$ and the second intermediate state with $1\Delta h\nu$.[19] In our case, tuning the photon energy causes the disappearance of the A2 peak for photon energies larger than 3.01 eV, by the overwhelming signal from the B1 peak. From the energy separations of 0.41eV between A1 and A2, as well as between B1 and B2, which do not change with photon energy, we can deduce that these features are related to the $n=1$ and 2 image-potential states, respectively.[5] As estimated from the final-state energies of peaks A1 and B1 and the known position of the $n=1$ image-potential state at 4.04 eV at $k_\parallel=0$,[5] peaks A1 and B1 correspond to separations of 2.91 and 3.11 eV from the $n=1$ image-potential state, respectively.

To further illustrate the unusual features of the 3PPE spectra, in Fig. 1 we also compare 3PPE spectra with 2PPE and 4PPE spectra, which have been shifted in energy to align the photoemission peaks from the occupied *d* bands. The top 2PPE spectrum taken from a cesiated Cu(001) surface at 110 K shows only a broad structure without the splitting seen in 3PPE. In a previous 2PPE study of the *d* bands for Cs/Cu(001) with even higher electron energy resolution (30 meV) and lower temperature (35 K) the distinct splitting found in Fig. 1 could not be resolved.[9] As will be explained in detail below, this is because 2PPE using photon energies near 3 eV is nonresonant with respect to the image-potential states. The absence of $k_\perp$ selectivity that is provided by a resonance causes a reduced energy-filtering effect with respect to the initial *d*-band states when compared to the resonant 3PPE excitation via an intermediate IP state. In contrast, the bottom 4PPE spectrum clearly displays the spin-orbit splitting with seemingly the same resolution as the 3PPE peaks taking into account the reduced statistics due to a diminished count rate by about four orders of magnitude.[16] This observation is consistent with the fact that the 4PPE process shown proceeds via the same intermediate states as the 3PPE process to which it is compared.

IV. DISCUSSION

A. Electronic band structure of copper

In order to interpret our experimental results, we show in Fig. 2 the relativistic band structure of copper for the *k*-space line relevant to emission along the surface normal of a Cu(001) surface (Δ line from Γ to X) according to the calculated band structure of Eckardt *et al.*[20] We indicate a three-

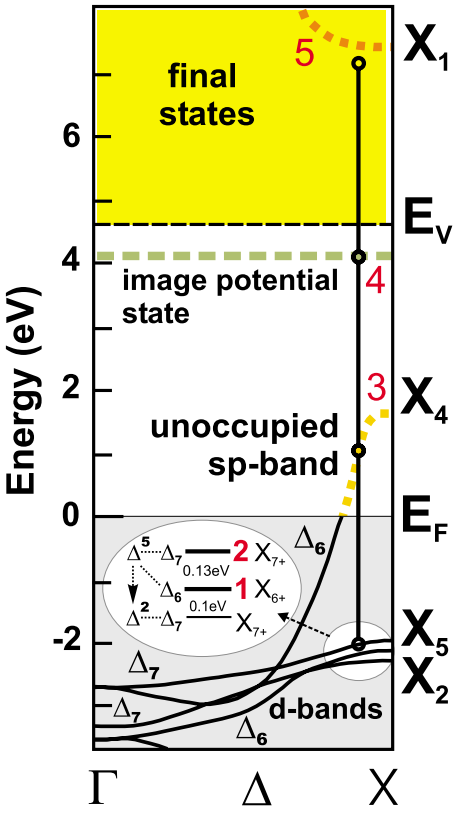

FIG. 2. (Color online) Relativistic band structure (Ref. 20) of Cu(001) with the proposed three-photon resonance for a photon energy near 3 eV. The final photoemitted states correspond to time-reversed low-energy electron diffraction states in the direction of the detector, with complex wave vectors in the band gap (Ref. 21).

photon process for photon energies near 3 eV starting from the Cu *d* bands via the unoccupied *sp* band and the $n=1$ image-potential state, which has been demonstrated previously.[16] This process was shown to be very effective, leading to a 3PPE signal higher in intensity than the simultaneously observed 2PPE signal, which occurs through nonresonant pathways.

As is well known, a theoretical band structure such as shown in Fig. 2 usually does not describe experimental photoemission data quantitatively.[22,23] Because of this, we assume in the following that the calculation still describes the *dispersion* of the bands correctly but we make the absolute values for the critical points adjustable to known experimental data. Then we try to find *k*-conserving resonances in the band structure as a function of photon energy. In a first approximation this is realized by shifting the involved bands according to the number of photons needed to reach the final-state energy. A strong resonance can be expected when the initial *d* bands, the intermediate *sp* bands and the image-potential state cross; this imposes very stringent conditions on the relative energy separation between the involved energy levels.

Adjusting the critical points, we took the position of X_4 at 1.8 eV (Refs. 24 and 25) and the *d* bands are assumed to have X_5 at −1.99 eV and X_2 at −2.18 eV.[22] Due to spin-orbit coupling, the Δ^5 band is split into Δ_7 and Δ_6 bands with reported experimental splittings between 100 (Ref. 26) and 170 meV (Ref. 27) in the region of interest near the X point. For comparison, the theoretical value is 160 meV (Ref. 22) at the X point. The intermediate image-potential states are taken at 4.04 eV for $n=1$ and at 4.45 eV for $n=2$.[5] The final *sp* band is assumed with X_1 at 7.67 eV (Ref. 22) and thus cannot be reached resonantly with the photon energies in our experiment. The initial state Δ^2 *d* band is neglected because of the selection rules for photoemission in the direction of the surface normal. The result of this shifting procedure for two-photon energies is shown in Fig. 3.

The results in Fig. 3 strongly support a resonance mechanism as responsible for the observed double-peak structure. As we show in Fig. 3, two different resonances are present for a pair of photon energies approximately 110 meV apart, at 2.97 and 3.08 eV. The corresponding 3PPE processes involve a two-photon resonance between one of the two *d* bands and the IP state and both are near one-photon resonance to unoccupied *sp*-band states. In view of the very simple model, both the photon energies and the separation of the resonances are in good agreement with the measured values. These resonances involve two initial states belonging to spin-orbit split Δ^5 *d* bands. They both proceed at different *k* values via the dispersing unoccupied portion of the *sp*-band states to the image-potential state. The IP state is a surface state which by definition does not show dispersion with momentum in the direction perpendicular to the surface and thus is drawn horizontally in the bulk band structure of Fig. 2. As can be seen by the position of the upper unoccupied *sp* band in Fig. 3 (dash dotted), a three-photon resonance involving final states from this band can be ruled out.

Our analysis also explains why the observed peaks do not shift according to the number of additional photons necessary to reach the final state when changing the center wavelength of the pulse. In the present case, the relatively broad frequency spectrum of the ultrashort pulse samples a range of resonance conditions. As long as the photon energies of the two most prominent resonance features are supplied by the pulse, there will only be a change in the relative peak amplitudes of the two features as the central photon energy of the pulse is tuned. This obviously shows that features A and B are not a consequence of the presence of the IP state alone but are inherently caused by a nonlinear resonance effect between initial, first intermediate states, and second intermediate (IP) states. Very qualitatively, a memory of its excitation pathway must be imparted on an electron because it starts at a specific energy level (one of the two *d* bands), then goes through the *same* energy level of the IP state as the other electrons and finally it ends up at a specific energy again. In this sequential picture where only the actual population of the IP state is measured by the third ionizing photon, no initial-state peaks could show up in the photoelectron spectrum if the electrons from different initial states lose memory of their excitation pathway in the IP state before their final ionization. In this respect, the simple observation of two IP-state-related peaks that do not move when the central pulse energy is tuned is a sign of specific nonlinear-optical pathways that cannot be pictured as sequential one-photon transitions but that allow the electron to keep its initial-state information as it is emitted into the vacuum.

The resonance effect also provides an effective energy filter, which would explain why the width of the observed

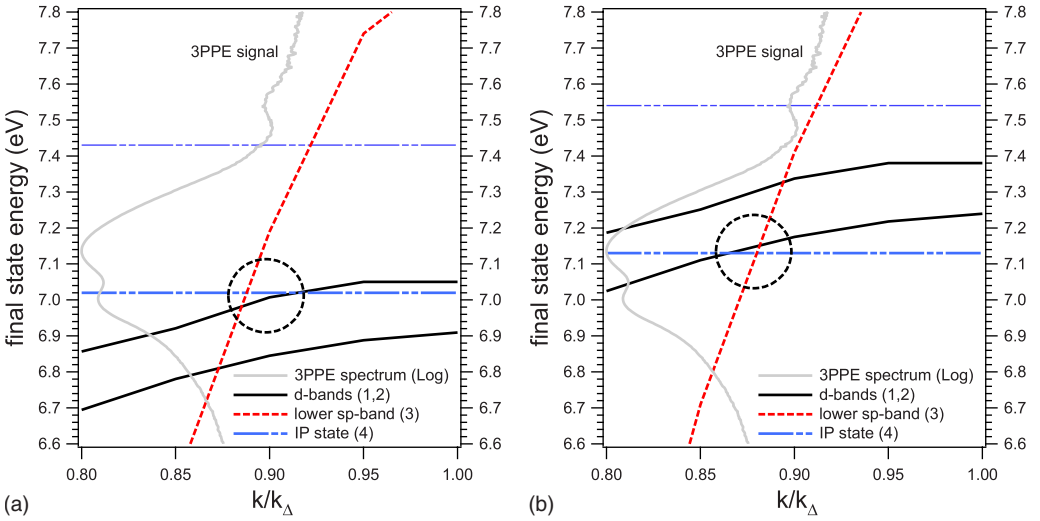

FIG. 3. (Color online) Estimation of resonance conditions for $h\nu$=2.97 eV (left) and $h\nu$=3.08 eV (right) by shifting initial and intermediate states according to the number of necessary photons to reach the final-state energy. The bands are numbered according to Fig. 2. The crossing of initial (solid black), first intermediate (dashed red), and second intermediate (dash-dot-dot, blue) state bands indicates simultaneous one-photon and two-photon resonances between one of the two d bands, the sp band, and the n=1 image-potential state. Due to the broad pulse spectrum (≈170 meV), the separate resonances connected to the two d bands are simultaneously observed in the experimental spectrum (solid gray, experimental data for 3.08 eV central photon energy of the laser pulse, compare with Fig. 1).

peaks A and B is smaller than the optical spectrum of the excitation pulses. Strictly, energy conservation is imposed only on the overall coherent 3PPE process from an initial to a final state that are separated by $\hbar\omega_3$. In principle all three-photon processes that fulfill $\hbar\omega_3=\hbar\omega_0+\hbar\omega_1+\hbar\omega_2$ are allowed. However, if we are additionally near one-photon resonances $\hbar\omega_R$ between dispersing levels (compare Fig. 3), energy conservation is also approximately fulfilled for the intermediate levels. This favors the photon energies near the simultaneous one-photon, two-photon, and three-photon resonances $\hbar\omega_3=\hbar(\approx\omega_R)+\hbar(\approx\omega_R)+\hbar(\approx\omega_R)$ and thus provides an energy-filtering mechanism.

B. Quantum mechanical model for three-photon photoemission

In order to gain a better insight into the observed three-photon photoemission processes, the above analysis has to be supplemented by a more quantitative theoretical model. Two-photon photoemission has been described in the density-matrix formalism, where the populations of the involved states are described by the diagonal elements ρ_{aa} and the coherences between states by the off-diagonal elements ρ_{ab} of the density matrix ρ.[5,14,28–31] The application to three-photon photoemission is straightforward but more involved due to the presence of more energy levels in the system. In order to clarify the nomenclature for the various electronic states and processes, we give the following explicit definitions which will be referred to in the discussion below.

We assume that the part of the Cu band structure that is relevant for the observed 3PPE process can be effectively simplified to a four-level system. The unperturbed Hamiltonian of the system is written in the basis of four orthonormalized states ($\langle a|b\rangle=\delta_{ab}$) representing either one of the initially occupied d-band states $|i_{1,2}\rangle$, the intermediate unoccupied sp-band $|s\rangle$, the image-potential state $|m\rangle$, and the final photoemitted state $|f\rangle$ at the respective energy levels $\epsilon_{i,s,m,f}$. In order to keep the treatment transparent, we also include the zero matrix elements,

$$\hat{H}_S=\begin{pmatrix} \epsilon_i & |i\rangle\langle i| & 0 & |i\rangle\langle s| & 0 & |i\rangle\langle m| & 0 & |i\rangle\langle f| \\ 0 & |s\rangle\langle i| & \epsilon_s & |s\rangle\langle s| & 0 & |s\rangle\langle m| & 0 & |s\rangle\langle f| \\ 0 & |m\rangle\langle i| & 0 & |m\rangle\langle s| & \epsilon_m & |m\rangle\langle m| & 0 & |m\rangle\langle f| \\ 0 & |f\rangle\langle i| & 0 & |f\rangle\langle s| & 0 & |f\rangle\langle m| & \epsilon_f & |f\rangle\langle f| \end{pmatrix}. \tag{1}$$

This simplification disregards the dispersion of the electronic states with crystal momentum **k** that is a major inhomogeneous contribution to 2PPE spectra[30] and it neglects the various interband and intraband relaxation mechanisms that would need to be part of a quantitative theory for a crystalline solid-state system. This could be handled, e.g., by introducing sets of k-dependent multilevel systems with appropriate couplings that represent the above effects.[30,32] We also assume weak perturbation of the system by the laser pulse, thereby excluding effects that are typically related to significant population transfers during the action of the pulse such as, e.g., Rabi oscillations.[33] The 3PPE processes proceed independently from either of the two different sets of initial d-band states $|i_{1,2}\rangle$, which are uncorrelated single-particle states. This allows us to treat two uncoupled four-level systems instead of a five-level system with two closely spaced initial states.

The density operator $\hat{\rho}$ of this simplified system explicitly expands as

$$\hat{\rho} = \begin{pmatrix} \rho_{ii} & |i\rangle\langle i| & \rho_{is} & |i\rangle\langle s| & \rho_{im} & |i\rangle\langle m| & \rho_{if} & |i\rangle\langle f| \\ \rho_{si} & |s\rangle\langle i| & \rho_{ss} & |s\rangle\langle s| & \rho_{sm} & |s\rangle\langle m| & \rho_{sf} & |s\rangle\langle f| \\ \rho_{mi} & |m\rangle\langle i| & \rho_{ms} & |m\rangle\langle s| & \rho_{mm} & |m\rangle\langle m| & \rho_{mf} & |m\rangle\langle f| \\ \rho_{fi} & |f\rangle\langle i| & \rho_{fs} & |f\rangle\langle s| & \rho_{fm} & |f\rangle\langle m| & \rho_{ff} & |f\rangle\langle f| \end{pmatrix},$$

$$\rho_{ii}(t=-\infty) = 1. \tag{2}$$

We emphasize that the matrix element ρ_{ii} is the only nonzero element in the ground state at time $t=-\infty$, representing the initial population of the relevant d-band state.

The matrix element ρ_{ff} determines the quantity we measure in the experiment: the (very small) population that is transferred to the final state by the ultrashort optical pulse. Initially, $\rho_{ff}=0$ and it can only become nonzero due to the coupling to the initial state via the intermediate states. This coupling is provided by the electric field $E(t)$ of the excitation pulse. For simplicity, we assume here that the most relevant couplings are between those states which are nearly a photon energy $\hbar\omega_p$ apart in the level scheme,

$$|i\rangle \overset{\hbar\omega_p}{\leftrightarrow} |s\rangle \overset{\hbar\omega_p}{\leftrightarrow} |m\rangle \overset{\hbar\omega_p}{\leftrightarrow} |f\rangle. \tag{3}$$

In the density-matrix formalism, this specific coupling is achieved by retaining only the relevant matrix elements in the corresponding interaction Hamiltonian H_{int}, with the dipole moments μ_{ab} describing the relative strength of the coupling of $|a\rangle$ and $|b\rangle$ due to the presence of a classical electric field with amplitude $E(t)$ [polarization effects can be included by vectors $\vec{E}(t)$ and $\vec{\mu}_{ab}$],

$$\hat{H}_{\mathrm{int}}(t) = -E(t)\cdot \begin{pmatrix} 0 & |i\rangle\langle i| & \mu_{is} & |i\rangle\langle s| & 0 & |i\rangle\langle m| & 0 & |i\rangle\langle f| \\ \mu_{is}^{*} & |s\rangle\langle i| & 0 & |s\rangle\langle s| & \mu_{sm} & |s\rangle\langle m| & 0 & |s\rangle\langle f| \\ 0 & |m\rangle\langle i| & \mu_{sm}^{*} & |m\rangle\langle s| & 0 & |m\rangle\langle m| & \mu_{mf} & |m\rangle\langle f| \\ 0 & |f\rangle\langle i| & 0 & |f\rangle\langle s| & \mu_{mf}^{*} & |f\rangle\langle m| & 0 & |f\rangle\langle f| \end{pmatrix}. \tag{4}$$

For a solid-state system, the internal light field that gives rise to photoemission is influenced by the collective optical response of the system, which can be taken into account by a complex response function in the frequency domain.[34]

Starting at $t=-\infty$ from only $\rho_{ii}\neq 0$, the interaction Hamiltonian allows finite values to develop in the matrix elements during the time evolution of the density operator $\hat{\rho}$. This time evolution is described by the equation of motion for the density matrix (Liouville-von Neumann equation),[5,14,28,29,35]

$$\frac{d\rho_{ab}}{dt} = -\frac{i}{\hbar}\langle a|[\hat{H}_S + \hat{H}_{\mathrm{int}}, \hat{\rho}]|b\rangle - \Gamma_{ab}\rho_{ab} \quad (a,b = i,s,m,f). \tag{5}$$

Straightforward replacement of the definitions (1), (2), and (4) in Eq. (5) results in a set of coupled differential equations for the density-matrix elements ρ_{ab} which in principle can be numerically integrated using standard algorithms.

In Eq. (5), the Γ_{ab} are phenomenological parameters which are introduced to account for the relaxation of the system back to equilibrium by energy and momentum exchange with external degrees of freedom. In our simple picture we assume that the Γ_{ab} are constants, which leads to exponential decay behavior via the structure of Eq. (5) looking like $\dot{\rho}\propto -\Gamma\rho$. Qualitatively, much more complicated dynamics of the excited system can result if the electronic energy levels, the dipole moments, and decay rates themselves are functions of other degrees of freedom coupled to the system.[36]

The off-diagonal elements, i.e., the coherences ρ_{ab}, decay due to the influence of the population loss rates Γ_{aa} and Γ_{bb} of both involved levels and, in addition, the ρ_{ab} can decay due to the randomization of the relative quantum-mechanical phase between the states $|a\rangle$ and $|b\rangle$. In general, the coherences ρ_{ab} account for interference effects in the coupling between states $|a\rangle$ and $|b\rangle$, which will be washed out when the phase correlation of the oscillating dipole μ_{ab} between interactions with $E(t)$ at points in time t_1 and t_2 decays to zero.

The integrated dipole moment of an ensemble of dipoles can decay due to disappearance of dipoles from the ensemble (population loss rates Γ_{aa} and Γ_{bb}) but is also destroyed by phase randomization between dipoles that continue with the same strength of the oscillations but with increasingly random phases. On the single dipole level, the required phase jumps can happen if the quantum-mechanical superposition of $|a\rangle$ and $|b\rangle$ that created the dipole is changing its internal phase by, e.g., momentum scattering. The contribution that is solely due to the phase randomization (as opposed to population loss) is assumed to proceed with an exponential decay rate Γ_{ab}^{pd} determined by the interactions with the bath degrees of freedom ("pure dephasing," supposed to be composed of contributions that can be ascribed to both involved states separately like $\Gamma_{ab}^{pd}=\Gamma_{a}^{pd}+\Gamma_{b}^{pd}$),

$$\Gamma_{ab} = \Gamma_{ab}^{pd} + \frac{1}{2}(\Gamma_{aa} + \Gamma_{bb}). \tag{6}$$

As stated above, with the above definitions, the nonlinear photoemission signal proportional to ρ_{ff} can in principle be obtained by numerically integrating the coupled differential Eq. (5). We note here that the interaction is completely described by a *classical* electric field $E(t)$ and the notion of "n-photon processes" actually does not appear anywhere directly in the formalism we have discussed. The nonlinearities with respect to the intensity of the incident light appear due

to the mathematical properties of a system of coupled differential equations like the system [Eq. (5)] and *not* because any quantization of energy exchange is involved directly anywhere in the formalism.

The photoemission signal $N(E_f)$ at the final-state energy E_f is formally obtained from the population in the final state ρ_{ff} integrated over time (for finite pulse lengths) according to the standard procedure[14,37] of taking the trace of the operator of the relevant observable $|f\rangle\langle f|$ applied to $\hat{\rho}(t,E_f)$,

$$N(E_f) = \int_{-\infty}^{+\infty} dt\ \mathrm{Tr}\{|f\rangle\langle f|\hat{\rho}(t,E_f)\}. \tag{7}$$

For comparison, we note that electromagnetic signals observed in purely optical measurements originate from the induced material polarization $\vec{P}$ as a source term in the Maxwell equations. The polarization is related to the expectation value of the dipole operator $\hat{\mu}$: $\vec{P}=\mathrm{Tr}[\hat{\mu}\hat{\rho}]$. Because the dipole operator expands into matrix elements of the type $|b\rangle\langle a|$ (for two generic basis states $|a\rangle$ and $|b\rangle$),[35] it probes coherences between states (i.e., it measures the off-diagonal elements ρ_{ab}). The above treatment also illustrates how simultaneous nonlinear-optical and multiphoton photoemission experiments from the same system using the same laser source can be analyzed in a unified manner. Such combined experiments can provide additional information about the optically excited system under investigation.[38]

The numerical treatment of Eq. (5) is in principle straightforward. However, with respect to the physical interpretation, a perturbative expansion of $\hat{\rho}$ with respect to interactions with the electrical field is useful. Then the order of nonlinearity of the observed quantity as a function of the incident light field $E(t)$ can be determined. Such a perturbative expansion allows us to visualize the induction of nonzero matrix elements ρ_{ab} as a sequence of steps in which the commutators $[H_{\mathrm{int}},\rho_{ab}]$ in Eq. (5) are recursively expanded up to a specified order. This expansion can represented by double-sided Feynman diagrams which keep track of both the time development of the population in the involved states as well as the induced coherences between these states that are, respectively, described by the diagonal and off-diagonal elements of the density matrix.[35] Another related visualization allows us to show the possible coupling of two generic elements ρ_{ab} and ρ_{cd} of the density matrix as Liouville space pathways.[35]

These Liouville space pathways show that besides the sequential one-photon pumping of population from one state to the next [compare relation (3)],

$$\rho_{ii} \rightarrow \rho_{ss} \rightarrow \rho_{mm} \rightarrow \rho_{ff}, \tag{8}$$

there are contributions to ρ_{ff} containing only coherences, schematically written like

$$\rho_{ii} \rightarrow \rho_{is} \rightarrow \rho_{im} \rightarrow \rho_{if} \rightarrow \rho_{ff}, \tag{9}$$

which implies that these contributions produce no population in the intermediate states $|m\rangle$ (corresponding to the observable $N_m=\mathrm{Tr}[|m\rangle\langle m|\hat{\rho}]$) due to the fact that the density-matrix components ρ_{mm} are not affected by these processes. It is emphasized that despite the fact that no population in the intermediate state is involved, these states nevertheless have a decisive role. They contribute via their coherent superposition with the other states. From our experimental data, we see that the coherent coupling of the *d*-band states to the image-potential state via the *sp* bands contributes to the initial-state peaks in the photoelectron spectrum $[\rho_{ff}(E)]$. We keep in mind that the pathways (8) and (9) are two particular pathways in a general coherent 3PPE process and occur together with all other pathways and should be added coherently in calculating $\rho_{ff}(E)$.

C. Model calculations

As we discussed above, the theoretical modeling of our spectra requires the treatment of a number of four-level systems at different k points in the Cu band structure. Numerical integration of the corresponding set of Liouville-von Neumann equations would need realistic dipole matrix elements and relaxation rates of the relevant states, including their dispersion and possible intraband and interband interactions. However, the main physics of the effect to be explained is expected to be already present in three-level systems of initial, intermediate, and final states. For these systems, analytical solutions exist for single-frequency interactions in two-photon photoemission.[13] Assuming that the two initial *d*-band levels and the intermediate IP state play a dominant role in the mechanism we focus on here, we can simplify our four-level system (3PPE) to a three-level system (2PPE) by artificially moving the two initial *d*-band states to the original energy level of the first intermediate *sp* bands, which are neglected in the following. The neglect of the *sp* bands seems to be justified in this case since they are strongly dispersing and should not contribute significant additional spectral structure by themselves. The validity of this assumption would have to be checked in a quantitative theory since the *sp* bands can contribute additional intraband relaxation channels. We then apply the model of Wolf *et al.*[13] to our special simplified system that models 2PPE from two closely spaced, independent initial states via the same intermediate state. We assume a broad continuum of excitation frequencies and analyze how the resonance frequencies can be distinguished in the photoelectron spectrum, similar to transitions in an absorption spectrum using a broadband light source.

For the intermediate state we assumed a constant lifetime of 35 fs and a dephasing rate of 1 meV.[5] For the final state we assumed infinite population lifetime and 1 meV dephasing rate.[5] The initial states are separated by 150 meV, at energy levels that reproduce the experimentally observed final-state positions via the intermediate state at 4.04 eV, corresponding to the $n=1$ IP state on Cu(001). We then calculated the resulting 2PPE spectra for a range of initial-state dephasing rates (assuming no population decay in the initial state). The resulting 2PPE spectra in two-dimensional plots for photon energies ranging are shown in Fig. 4. We can distinguish two different linear dispersions, one with a slope of $2\Delta h\nu$, corresponding to the initial states and the other with a slope of $1\Delta h\nu$, corresponding to the intermediate state. Starting with dephasing times between 10 and 20 fs, the two

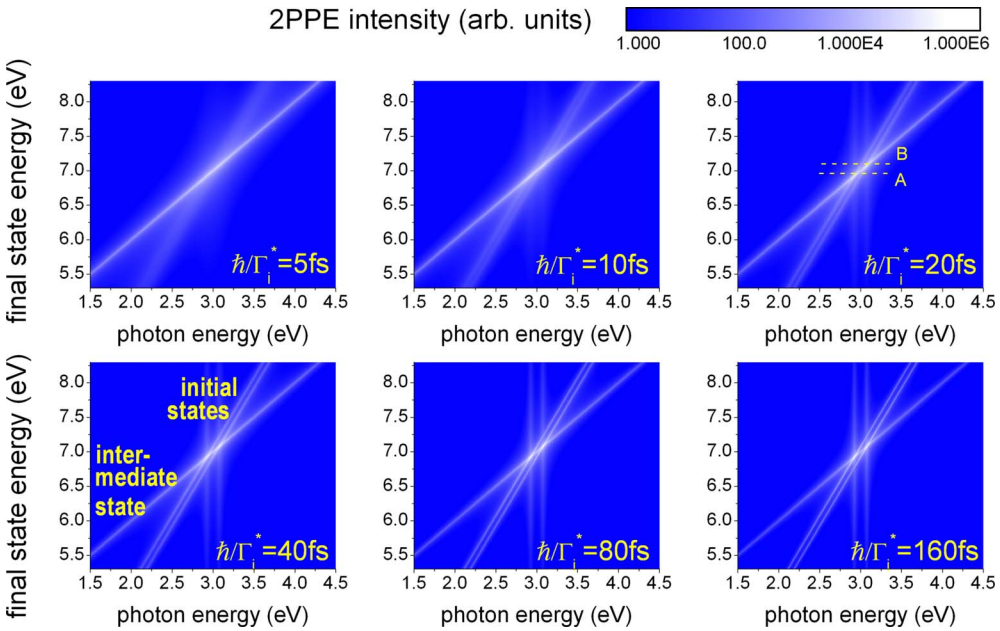

FIG. 4. (Color online) Simulations of one-color 2PPE from two closely spaced initial states via the same intermediate state for a continuous flat excitation spectrum with single-photon energies from 1.5 to 4.5 eV. The panels show the final-state 2PPE yield (logarithmic scale) as a function of the photon energy and final-state energy. The initial and intermediate-state peaks can be distinguished by the change in their final-state energy as a function of the photon energy $h\nu$ (initial state: $2\Delta h\nu$ and intermediate state: $1\Delta h\nu$). The two vertical lines (best visible in the lower panels) indicate the presence of two energy-filtering resonances A and B that increase the *absolute* intensity in the photoelectron spectra for the respective photon energies. The corresponding peak positions in the photoelectron spectrum are shown at A and B. The total photoelectron spectrum for the 3 eV broad continuum of incident light is obtained by integrating over the horizontal axes. With increasing dephasing time, the total photoelectron spectrum evolves from a single broad peak (5 fs) to two separate peaks (>10 fs) (see Fig. 5). In each panel, the assumed initial-state pure dephasing times are indicated. For the intermediate state, a population lifetime of 35 fs and a pure dephasing of 1 meV was assumed. In the final state, we took an infinite population lifetime and pure dephasing rate of 1 meV. The separation of the initial states is 150 meV.

initial states become separately visible. For faster dephasing, only a single peak is present.

Assuming a flat excitation spectrum ranging from 1.5 to 4.5 eV, the partial spectra for each energy were added to simulate the effect of a broad excitation spectrum. The result, corresponding to an average along the horizontal axis of Fig. 4, is shown in Fig. 5. Depending on the initial-state dephasing rate, we can observe a single broad peak or two separate peaks resolving the two initial states. This result for a model 2PPE process shows how the dephasing rate between initial state and intermediate state contributes to the peak width of the transition. If the dephasing rate is high, the two independent transitions from the closely spaced initial sates are broadened to an extent that they are not separable anymore and appear as a single peak. With decreasing dephasing, the peak widths of the two resonances become sharp enough to give two peaks in the final-state spectrum. This process can be expected to be of very general character and a similar influence of dephasing is expected to be relevant in the 3PPE experiment. This means that a sufficiently low dephasing rate of the initial states with respect to the intermediate states will be required in any case to distinguish two initial-state peaks in a transition that proceeds via a common intermediate-state level, such as the IP state considered here.

With respect to the 2PPE model calculation, the pure dephasing on one hand is almost totally due to the initial state since image-potential states on perfect surfaces can be assumed in good approximation to have a nearly zero pure dephasing rate:[5,12] $\Gamma_b^{pd} \approx 0$. The dephasing due to population decay on the other hand stems solely from the image-potential state since the initial states are assumed not to decay: $\Gamma_{ii}=0$. In the model calculation, an initial-state dephasing time of at least 10–20 fs is necessary for the observation of the separated peaks. Although this value cannot be taken

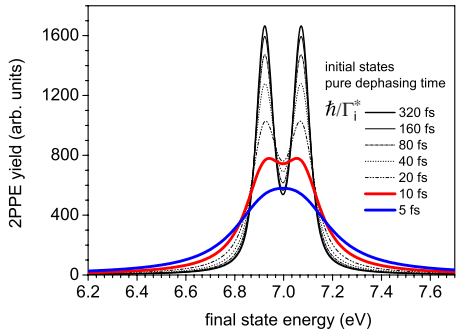

FIG. 5. (Color online) Summation of the spectra from Fig. 4 for all photon energies of the excitation continuum to simulate the total photoelectron spectrum. The presence of two resonances can be clearly distinguished. While the underlying initial and intermediate-state features disperse with photon energy, they strongly change their intensity (logarithmic scale in Fig. 4) to result in the resonance peaks in the total sum spectra shown above. An instrumental broadening of 50 meV was assumed.

as a completely quantitative estimation, nevertheless it compares well with direct time-domain observations of Cu *d*-band hole dephasing times of >20 fs in the observed *d*-band region near the X point.[9]

For ultrashort pulses, the optical frequencies are not independent of each other and this coherent excitation spectrum will additionally have an influence on the observed photoelectron spectra. We assume that a coherent broad pulse spectrum would still tend to broaden the photoelectron peaks rather than to make them narrower in comparison to single-frequency excitation (the actual amount of broadening can be limited by the resonant energy-filtering process discussed above). Other influences such as the dispersion of the involved electronic bands also would lead to an additional broadening. This implies that the observed experimental width of the peaks in the 3PPE spectrum is an upper limit estimation when compared to the results from the simplified 2PPE model. This is why the above estimations based on a single-frequency and continuous-wave approximation should in any case present lower limits on the dephasing times compatible with the observation of two separate peaks in the 3PPE spectrum.

V. CONCLUSION AND SUMMARY

Our observations of the direct influence of coherent excitation pathways in 3PPE from Cu(001) are relevant for applications of nonlinear photoemission in electronic structure investigations, which can be carried out using high-intensity laboratory laser sources and synchrotron-based free-electron lasers. It has been predicted theoretically[15] that resonant two-photon photoemission could give the separation between occupied initial states and unoccupied intermediate *bulk* states within the fundamental limit imposed by the intrinsic energy and momentum widths of the coupled states. The important advantage in such two-photon measurements is that the optical transition from the initial state to the intermediate state would couple bulk states which are not influenced by the symmetry breaking due to the surface[39] and the perpendicular crystal momentum $k_\perp$ in such a transition would need to be conserved (at negligible photon momentum). The extension of this idea to 3PPE is straightforward and we illustrate in Fig. 6 the qualitative difference between unspecific bulk excitations and coherent resonances which sensitively depend on the band dispersion. It can also be easily imagined that this approach can be generalized to multiple excitation frequencies which can be tuned to search for the simultaneously possible single-photon resonances in a multiphoton process. Furthermore, the use of multiphoton resonances corresponding to very well-defined *k*-space positions should allow improved time-domain investigations[6] of band-resolved electron dynamics. The demonstrated coherent coupling of bulk states to surface states through a two-photon resonance could also lead to improved possibilities of controlling electron motion at surfaces by interferometric techniques.[10,40]

In summary, we have demonstrated the clear influence of coherent excitation pathways in three-photon photoemission from Cu(001). Our findings suggest extensions to future studies of bulk band structure with tuneable laboratory and free-electron laser sources, exploiting multiphoton resonances for band mapping. If we note that when—in addition to the energy of the exciting radiation—the quantum-mechanical phase relationships between the coupled states and the radiation also become a defining factor in the nonlinear excitation process,[7] qualitatively different applications as compared to conventional band mapping with one-photon ARPES are expected by exploiting the unique properties of multiphoton transitions between occupied and unoccupied bulk states.

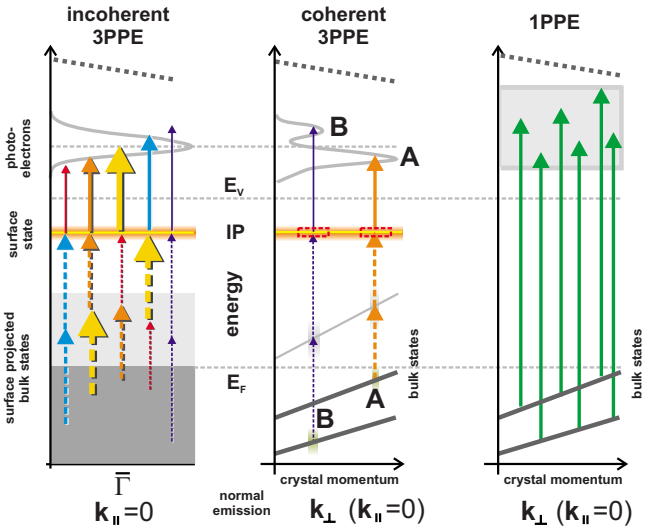

FIG. 6. (Color online) Principle of detecting coherent bulk band-structure resonances in 3PPE via an image-potential state on Cu(001). Left: nonresonant incoherent excitation of the IP state from unspecific bulk bands at normal emission ($k_\parallel=0$). The initial states are averaged over $k_\perp$ illustrating the loss of $k_\perp$ information in the sequential one-photon pathways due to the total lack of a $k_\perp$ selection rule in the IP to final-state one-photon transition ($k_\perp$ is undefined for surface states). The colors of the arrows correspond to photon frequencies provided by the excitation pulse, their thickness corresponds to the respective spectral weight. The photons can act in any combination for sequential incoherent excitations. The peak position of the IP state is determined by the central photon energy of the pulse (thickest arrow) and the measured width of the IP state is determined by the width of the pulse spectrum. Middle: coherent 3PPE resonances in the bulk band structure coupled to the image-potential state produce specific peaks A and B in the spectrum, providing $k_\perp$ information. A fixed photon energy defines each resonant pathway. The width of features A and B is not limited by the spectral pulse width. Right: the corresponding 1PPE process for the same level scheme using a single-photon energy of $\approx 3h\nu_{3\mathrm{PPE}}$ is less *k* selective if no resonance to a dispersing final-state band is present (e.g., off-resonant transition to final band broadened by absorption).

ACKNOWLEDGMENTS

We thank Frank Helbig for invaluable technical support. H.P. is grateful for support by NSF under Grant No. CHE-0650756.

*winkelm@mpi-halle.mpg.de

[1] A. Einstein, Ann. Phys. **322**, 132 (1905).

[2] *Solid-State Photoemission and Related Methods: Theory and Experiment*, edited by W. Schattke and M. A. Van Hove (Wiley-VCH, Weinheim, 2003).

[3] S. Hüfner, *Photoelectron Spectroscopy* (Springer-Verlag, Berlin, New York, 1995).

[4] Th. Fauster, *Solid-State Photoemission and Related Methods: Theory and Experiment* (Ref. 2), pp. 247–268.

[5] M. Weinelt, J. Phys.: Condens. Matter **14**, R1099 (2002).

[6] H. Petek and S. Ogawa, Prog. Surf. Sci. **56**, 239 (1997).

[7] H. Petek, A. P. Heberle, W. Nessler, H. Nagano, S. Kubota, S. Matsunami, N. Moriya, and S. Ogawa, Phys. Rev. Lett. **79**, 4649 (1997).

[8] S. Ogawa, H. Nagano, H. Petek, and A. P. Heberle, Phys. Rev. Lett. **78**, 1339 (1997).

[9] H. Petek, H. Nagano, and S. Ogawa, Phys. Rev. Lett. **83**, 832 (1999).

[10] J. Güdde, M. Rohleder, T. Meier, S. W. Koch, and U. Höfer, Science **318**, 1287 (2007).

[11] U. Höfer, I. L. Shumay, C. Reuss, U. Thomann, W. Wallauer, and T. Fauster, Science **277**, 1480 (1997).

[12] T. Fauster, M. Weinelt, and U. Höfer, Prog. Surf. Sci. **82**, 224 (2007).

[13] M. Wolf, A. Hotzel, E. Knoesel, and D. Velic, Phys. Rev. B **59**, 5926 (1999).

[14] S. Ramakrishna and T. Seideman, J. Chem. Phys. **122**, 084502 (2005).

[15] W. Schattke, E. E. Krasovskii, R. Díez Muiño, and P. M. Echenique, Phys. Rev. B **78**, 155314 (2008).

[16] F. Bisio, M. Nývlt, J. Franta, H. Petek, and J. Kirschner, Phys. Rev. Lett. **96**, 087601 (2006).

[17] A. Winkelmann, F. Bisio, R. Ocana, W.-C. Lin, M. Nývlt, H. Petek, and J. Kirschner, Phys. Rev. Lett. **98**, 226601 (2007).

[18] A. Winkelmann, W.-C. Lin, F. Bisio, H. Petek, and J. Kirschner, Phys. Rev. Lett. **100**, 206601 (2008).

[19] W. Steinmann, Phys. Status Solidi B **192**, 339 (1995).

[20] H. Eckardt, L. Fritsche, and J. Noffke, J. Phys. F: Met. Phys. **14**, 97 (1984).

[21] R. Courths, H. Wern, G. Leschik, and S. Hüfner, Z. Phys. B: Condens. Matter **74**, 233 (1989).

[22] V. N. Strocov, R. Claessen, F. Aryasetiawan, P. Blaha, and P. O. Nilsson, Phys. Rev. B **66**, 195104 (2002).

[23] V. N. Strocov, R. Claessen, G. Nicolay, S. Hüfner, A. Kimura, A. Harasawa, S. Shin, A. Kakizaki, H. I. Starnberg, P. O. Nilsson, and P. Blaha, Phys. Rev. B **63**, 205108 (2001).

[24] J. E. Ortega, F. J. Himpsel, G. J. Mankey, and R. F. Willis, Phys. Rev. B **47**, 1540 (1993).

[25] A. Mugarza, A. Marini, T. Strasser, W. Schattke, A. Rubio, F. J. García de Abajo, J. Lobo, E. G. Michel, J. Kuntze, and J. E. Ortega, Phys. Rev. B **69**, 115422 (2004).

[26] C. M. Schneider, J. J. Demiguel, P. Bressler, P. Schuster, R. Miranda, and J. Kirschner, J. Electron Spectrosc. Relat. Phenom. **51**, 263 (1990).

[27] R. Courths and S. Hüfner, Phys. Rep. **112**, 53 (1984).

[28] E. Knoesel, A. Hotzel, and M. Wolf, J. Electron Spectrosc. Relat. Phenom. **88-91**, 577 (1998).

[29] H. Ueba and T. Mii, Appl. Phys. A: Mater. Sci. Process. **71**, 537 (2000).

[30] M. J. Weida, S. Ogawa, H. Nagano, and H. Petek, J. Opt. Soc. Am. B **17**, 1443 (2000).

[31] N. Pontius, V. Sametoglu, and H. Petek, Phys. Rev. B **72**, 115105 (2005).

[32] T. Meier, P. Thomas, and S. W. Koch, *Coherent Semiconductor Optics* (Springer, New York, 2007).

[33] L. C. Allen and J. H. Eberly, *Optical Resonance and Two-Level Atoms* (Dover, New York, 1988).

[34] M. Merschdorf, C. Kennerknecht, and W. Pfeiffer, Phys. Rev. B **70**, 193401 (2004).

[35] S. Mukamel, *Principles of Nonlinear Optical Spectroscopy* (Oxford University Press, New York, 1995).

[36] An example would be the optical excitation electrons at a surface, inducing nuclear motion of an adsorbate atom, leading to shifting *electronic* energy levels and changing wave function overlap, causing changes in the dipole moments and electronic transition rates, and finally feeding back onto the induced *nuclear* motion in the next time step (Ref. 41). Inclusion of such processes would introduce additional nonlinear character into the system of Eq. (5).

[37] H. Ueba and B. Gumhalter, Prog. Surf. Sci. **82**, 193 (2007).

[38] F. Bisio, A. Winkelmann, W.-C. Lin, C.-T. Chiang, M. Nývlt, H. Petek, and J. Kirschner, Phys. Rev. B **80**, 125432 (2009).

[39] V. N. Strocov, J. Electron Spectrosc. Relat. Phenom. **130**, 65 (2003).

[40] J. Gauyacq and A. Kazansky, Appl. Phys. A: Mater. Sci. Process. **89**, 517 (2007).

[41] H. Petek, M. J. Weida, H. Nagano, and S. Ogawa, Science **288**, 1402 (2000).